HHS Public Access

Author manuscript

*ACS Appl Bio Mater*. Author manuscript; available in PMC 2022 April 19.

Published in final edited form as:

*ACS Appl Bio Mater*. 2021 April 19; 4(4): 3639–3648. doi:10.1021/acsabm.1c00134.

# An Elastic Mineralized 3D Electrospun PCL Nanofibrous Scaffold for Drug Release and Bone Tissue Engineering

**Jacob Miszuk**[a], **Zhipeng Liang**[b], **Jue Hu**[a], **Hanna Sanyour**[c], **Zhongkui Hong**[c], **Hao Fong**[b,*], **Hongli Sun**[a,**]

[a]Department of Oral and Maxillofacial Surgery, Iowa Institute for Oral Health Research, University of Iowa College of Dentistry, Iowa City, IA 52242, USA

[b]Program of Biomedical Engineering, South Dakota School of Mines and Technology, Rapid City, SD 57701, USA

[c]Department of Biomedical Engineering, University of South Dakota, BioSNTR, Sioux Falls, SD 57107, USA

## Abstract

Complex shaped and critical-sized bone defects have been a clinical challenge for many years. Scaffold-based strategies such as hydrogels provide localized drug release while filling complex defect shapes, but ultimately possess weaknesses in low mechanical strength alongside a lack of macroporous and collagen-mimicking nanofibrous structures. Thus, there is a demand for mechanically strong, extracellular matrix (ECM) mimicking scaffolds that can robustly fit complex shaped critical sized defects and simultaneously provide localized, sustained, multiple growth factor release. We therefore developed a composite, bi-phasic PCL/hydroxyapatite (HA) 3D nanofibrous (NF) scaffold for bone tissue regeneration by using our innovative electrospun-based thermally induced self-agglomeration (TISA) technique. One intriguing feature of our ECM-mimicking TISA scaffolds is that they are highly elastic and porous even after evenly coated with minerals and can easily be pressed to fit different defect shapes. Furthermore, the bio-mimetic mineral deposition technique allowed us to simultaneously encapsulate different type of drugs, e.g., proteins and small molecules, on TISA scaffolds under physiologically mild conditions. Compared to scaffolds with physically surface-adsorbed phenamil, a BMP2 signaling agonist, incorporated phenamil composite scaffolds indicated less burst release and longer lasting sustained release of phenamil with subsequently improved osteogenic differentiation of cells in vitro. Overall, our study indicated that the innovative press-fit 3D NF composite scaffold may be a robust tool for multiple-drug delivery and bone tissue engineering.

## Graphical Abstract

[*]**Corresponding Authors**: Professor Hao Fong, Ph.D., Tel.: +1 605-394-1229; Fax: +1 605-394-1232; Hao.Fong@sdsmt.edu.
[**]**Corresponding Authors**: Professor Hongli Sun, Ph.D., Tel.: +1 319-335-1217; Fax: +1 319-335-8895; Hongli-Sun@uiowa.edu.

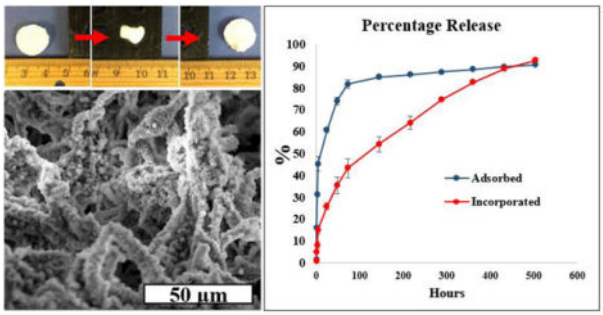


**Keywords**

Drug Release; Press-fit; 3D Electrospun Nanofibrous scaffold; Composite Scaffold; Bone Tissue Engineering

## 1. Introduction

Critical sized bone defects present a significant clinical challenge for bioengineered scaffold matrices due to their large sizes and often complex shapes.[1, 2] Graft-replacement techniques suited to fill irregular defects include strategies such as 3D printing and hydrogel-based scaffolds. Newly emerging 3D printing techniques can custom-fit complex shaped defects[3], but these techniques have difficulties achieving nanofibrous structure as well as drug binding/release capacity as natural ECM, which are very important for the success of synthetic tissue engineered scaffolds.[4] Shape memory polymers (SMPs) are another class of materials able to uniquely fit irregular defects upon thermal treatment, however, require thermal treatment of materials post implantation.[5, 6] Additionally, SMPs have shown to be adaptable to electrospinning techniques, forming nanofibrous structures for bone tissue engineering.[7] The ability of SMPs to form biomimicking composites is not yet studied however, where mineral composites may compromise the memory-properties of these materials. Hydrogels are another well-studied material providing a natural ECM-mimicking 3D environment for cell penetration with ability to swell and conform to any complex defect shape.[8–11] However, most hydrogels face limitations in cell penetration and lack adequate mechanical strength for strong osteogenic integration.[12]

The innovative TISA technique described in our previous work has demonstrated capability of generating highly elastic, 3D NF structures with interconnected porous structure for bone tissue engineering.[13] One key characteristic of the TISA-generated scaffold is the high elasticity of the NF matrix, allowing it to be used as a press-fit strategy for defect replacement. Scaffolds without press-fit capabilities normally require fixation via glues or sutures, features that can cause damage to surrounding tissue or disrupt the regeneration process, and require additional procedures to remove or repair these fixtures.[14, 15] Press-fit scaffolds utilize high elasticity to robustly fit numerous complex defect shapes with minimal processing, and provide uniform and tight contact between scaffold material and host tissue, typically leading to better implant stability and success rate.[16] Additionally, high elastic strength allows for these scaffolds to be implanted in a minimally invasive manner due to their compressibility.[17] Compared to SMP-class materials, no thermal treatment is required

after implantation.[5, 6] Polycaprolactone (PCL) scaffolds inherently are severely hydrophobic, and mimic only the organic collagenous phase of natural bone ECM. One common technique to improve the osteogenic capability of biomaterials and to better mimic the natural ECM of bone is to develop composite materials with a synthetic mineral phase as other groups have done with numerous polymers.[18–20] To improve on the bioactivity of TISA-PCL scaffolds, we developed techniques including PCL/PLA blend polymers, and functionalized the surface/bulk of scaffolds with bone-like mineral hydroxyapatite (HA) and introduced small molecule phenamil as a BMP2 activator.[21–23] Improved bioactive TISA scaffolds showed marked improvements in osteogenic markers *in vitro* as well as improved new bone formation in a mouse cranial defect model.[22] One key factor that remains unexplored is biomaterials-based drug delivery strategies for localized and sustained release of growth factors key to guiding bone regeneration incorporated into the TISA-generated scaffolds.

As bone regeneration is a long, complex physiological process encompassing many stages and growth factors during repair, sustained, localized and multiple drug delivery is always desired for efficient biomaterials-based bone regeneration.[24, 25] Single-drug release strategies see limited improvements in induced regeneration, as endogenous bone repair is characterized by multiple factors over an extended period of time.[26, 27] A key and well-studied molecule family in the bone regeneration process are bone morphogenic proteins (BMP), where BMP2 and BMP7 are FDA-approved growths factor for biomaterials-based drug delivery.[28, 29] Despite their potent osteogenic-inducing capabilities, BMPs are highly cost-ineffective and have extremely short half-life in solution, leading new focus toward biomaterials-based sustained drug delivery platforms to protect and extend the release window of these molecules.[30, 31] Another small molecule, phenamil, has been shown to act as a BMP2 activator through signaling pathways, where it can enhance the effects of endogenous and administered BMPs for improved osteogenic differentiation of stem cells.[32–34] Our recent work with phenamil highlighted this small molecule's ability to synergistically enhance new bone formation when treated in parallel with hydroxyapatite-functionalized TISA-PCL scaffolds.[22] However, phenamil in high doses can cause adverse side effects including cytotoxicity, so it is critical to develop a sustained-dose release profile for effective bone tissue engineered scaffolds.[35]

In this work, we apply a two-step mineral modification technique to TISA-PCL scaffolds and analyze the resulting flexibility, elasticity and mechanical strength of scaffolds, while characterizing the sustained release of proteins and small molecule drugs and observing their effects on osteogenesis. We hypothesize that sustained release of small molecule from embedded HA crystals will significantly strengthen the osteogenic capabilities of scaffolds over single-dosage application, thereby lowering risk of high initial cytotoxic dosage and reducing need for repeat drug treatment during bone regeneration processes.

# 2. Experimental

## 2.1 Materials

Polycaprolactone (PCL, Mw=80,000), gelatin (G1890), ethanol, dichloromethane (DCM), and N,N-dimethylformamide (DMF) were purchased from Sigma-Aldrich (St. Louis, MO). All of the chemicals and materials were used without further purification

## 2.2 Electrospinning and scaffold fabrication

TISA scaffolds were synthesized as described in our previous work[13, 22]; PCL NF mats with diameter 10–200nm were generated via electrospinning process with a high-voltage power supply (Gamma High Voltage Research, Inc., Ormond Beach, FL) and a laboratory-produced roller (with diameter of 25cm). Individual NF were isolated after 2D mats were generated via mechanical grinding of mats in liquid nitrogen. The individual NF were immersed in a glass bottle into a water/gelatin/ethanol mixture (4/2/1 volume ratio, respectively) and submerged in a water bath at 55°C for 3 mins. During this step, the individual PCL NF spontaneously agglomerated into a 3D structure. Immediately after 3 min, the suspended NF inside glass vial was submerged into an ice water bath for 30 mins to prevent further shrinkage/agglomeration of NF. Finally, the newly-formed 3D agglomerate structure was rinsed with DI water several times to remove residual gelatin and ethanol, and then lyophilized for further experiment.

## 2.3 HA deposition by wet precipitation in simulated body fluid (SBF)

A two-step simulated body fluid method was used to deposit first an amorphous calcium phosphate “primer” layer, followed by a crystalline layer as previously described by Wu et. Al[36]. TISA-PCL scaffolds were cut into discs 5mm diameter, 2mm thickness by biopsy punch for treatment. Scaffolds were first immersed into a priming solution of five-fold simulated body fluid with following molar concentrations; 684 mM NaCl, 12.5 mM $CaCl_2$,·$2H_2O$, 5mM $Na_2HPO_4$·$2H_2O$, and 21 mM $NaHCO_3$ for 24h at 37°C, shaking at 120rpm. For confocal imaging purposes, rhodamine B was introduced into this solution at concentration of 0.1mg/mL. Scaffolds were removed from the solution, rinsed briefly with DI water to remove excess ions and subsequently lyophilized before the second treatment step. Scaffolds were then immersed in a supersaturated solution of calcium phosphate with following molar concentrations; 40mM HCl, 4 mM $CaCl_2$,·$2H_2O$, 136 mM NaCl, and 2mM $Na_2HPO_4$·$2H_2O$, buffered to pH 7.4 with Tris, for 48h at 37°C, shaking at 120rpm. Drug/protein incorporation into this phase was done with BSA at 0.1 mg/mL, or phenamil at 0.2 mg/mL.

## 2.4 Surface and morphological characterization

A Zeiss Supra 40VP field-emission scanning electron microscope (SEM) was utilized to characterize morphological features of scaffolds prior to and after each step of treatment by SBF. Scaffolds were sputter coated with gold for 60s prior to imaging by SEM, and imaged in high vacuum mode at 5–30kV. Water contact angle was determined by VCA Optima goniometer and imaged with VCA OptimaXE software (AST Products Inc.). Scaffolds were immobilized horizontally on glass surface where a 2.0 μL water droplet was rested on the

surface for 10s before images were taken and contact angle was determined. Surface chemical compositions were analyzed before treatment and after each step of SBF immersion and after freeze-drying via attenuated total reflectance (ATR) spectroscopy (Nicolet, USA). Spectroscopies were obtained from 400 0$cm^{-1}$ to 400$cm^{-1}$.

### 2.5 Mechanical Testing

The atomic force microscope (AFM, Model: MFP-3DBIO, Asylum Research, Santa Barbara, CA) mounted on an inverted microscope (Model: IX73, Olympus America Inc.) was used to quantify the elastic modulus of the electrospun material. A silicon nitride tip (0.6 N/m) (MLCT-O10, Bruker, Santa Barbara, CA) attached with a 5μm glass sphere was used to indent the electrospun fibrous material at an indentation speed of 1μm/s. Each sample was probed at three different locations and measured. The fibrous material Young's modulus was estimated by fitting a modified Hertz model onto the AFM indentation curve using the built-in function of AFM software (Asylum Research).

### 2.6 Protein and small molecule release

TISA/HA Composite scaffolds were studied for *in vitro* bovine serum albumin (BSA) and phenamil release. For adsorbed drug/protein comparison, 100 μg of BSA or phenamil were dropped in aqueous solution onto scaffolds and then immediately lyophilized. Freeze-dried scaffolds were immersed in 1mL of PBS solution at 37°C. Each sample was incubated in an orbital shaker (Thermo Scientific, Waltham, MA), shaking at 120rpm. PBS was exchanged and collected at various intervals up to 21 days, where amount released was determined by BCA protein kit (Thermo Scientific) for protein, and via UV spectrometry for phenamil, at an absorbance of 366nm. Fluorescence imaging for release and drug incorporation 3D study was done by Olympus FV1200 confocal microscope.

### 2.7 *In vitro* cell study

**2.7.1 Cell Morphology—**C2C12 morphologies on different scaffolds were visualized by Texas red-X phalloidin (Molecular Probes, Grand Island, NY) and DAPI (Southern Biotech, Birmingham, AL) staining methods, labeling F-actin and cell nuclei, respectively.[23, 37]

**2.7.2 ALP Activity—**ALP activity of C2C12 cells was analyzed by using an EnzoLyte pNPP Alkaline Phosphatase Assay Kit (AnaSpec, San Jose, CA).[38] Adherent cells were suspended in assay buffer supplemented with Triton X-100, which was subsequently transferred to a tube and centrifuged at 2500g at 4°C, where the lysate was collected and mixed with the p-nitrophenyl phosphate and incubated for 30min at 37°C. Immediately following incubation, the reaction was terminated with addition of stop solution as described in the manufacturer's manual, and absorbance was measured at 405nm. This activity was normalized against total protein content, which was measured by BCA protein kit (Thermo Scientific) according to manufacturer's instruction, absorbance being measured at 562nm after 30min of lysate incubation with the working solution from BCA kit.

**2.7.3 Gene Expression Analysis—**Total RNA of cells was isolated using a GeneJET™ RNA Purification Kit (Thermo Scientific) by following manufacturer's instruction. RNA concentration was determined by absorbance at 260nm, where an

equivalent amount of RNA per group was processed via High Capacity cDNA Reverse Transcriptase Kit (Applied Biosystems, Forster City, CA) to generate cDNA. Quantitative PCR (qPCR) was performed with Taqman gene expression assays (Applied Biosystems) GAPDH (Mm99999915), Runx2 (Mm00501584), and OCN (Mm03413826) as described in several of our previous works.[13, 22, 23]

**2.7.4 Statistical analysis—**Statistical significance of observed differences between study groups were determined by using a two-tailed homoscedastic t-test; where a value of $p < 0.05$ was considered to be statistically significant, while $0.05 < p < 0.10$ was considered to be non-significant but a clear trend in cell or tissue response.

## 3. Results

### 3.1 Morphology and surface characteristics of 2-step HA coating

The two-step HA deposition SBF method was first used on 2D electrospun mats to characterize bioactivity with contact angle goniometry and ATR spectroscopy. Figure 1 depicts surface morphology of electrospun fibers prior to SBF immersion (A), and after step 1 (B) and step 2 (C) SBF treatment. HA coating was ubiquitous and consistent across the entirety of the mats, indicating great ease of the precipitation method. Wettability was measured to determine the change in hydrophobicity, where a significant decrease from 133° down to 4° and complete adsorption was noted from PCL only (Fig. 1A) to PCL with nucleated fibers (Fig. 1B) and full crystallization (Fig. 1C). The crystalline phase was examined via FTIR-ATR to determine surface chemical composition, where characteristic peaks of phosphate were readily apparent at 1040 and 600–560 (Fig. 1D), typical peaks of hydroxyapatite as noted in prior literature.[39]

### 3.2 Morphology of PCL/HA-3D scaffolds

Our previously SBF-modified TISA scaffolds utilized a single-step supersaturated calcium phosphate solution, yielding uniformly dispersed, microsphere-like HA crystals throughout scaffolds.[22] This work utilizes an initial ‘nucleation’ step, and a second ‘propagation’ step treatment for more nanofiber-localized coating. The electrospun PCL 3D-nanofibrous scaffolds with interconnected and hierarchically structured pores were characterized by SEM, prior to either step of SBF treatment (Fig.2A), after crystal nucleation (Fig. 2B), and after the final supersaturated calcium phosphate solution (Fig. 2C) at low (top panels Fig. 2) and high (bottom panels) magnifications. Compared to NF mats from Fig. 1, the highly porous morphology of the TISA allowed for deposition of HA on each individual nanofiber. After both steps of SBF treatment, pore interconnectivity was maintained throughout the scaffold while a uniform coating was deposited throughout the surface and cross-section of the scaffold, with an average diameter of 2.4 ±0.41 μm after treatment. Based on the SEM, after this even coating on the material the interconnected porous morphology was still not interrupted.

### 3.3 Mechanical testing and elasticity

Scaffold elasticity was demonstrated via compressing scaffolds into several complex shapes representing bone defect shapes for 10 minutes and then allowing to rest for 60sec after

removal (Fig. 3A–F). Both PCL and PCL/HA scaffolds re-expanded to >95% of their original diameters within 60s of removal from compression. Additionally, after removal from load, nanofiber/HA morphology remained unchanged as examined by SEM (Fig. 3G–H). The retained elasticity is interesting, and is possibly due to the coating layer being thin enough as to not interrupt the interconnected porous morphology of scaffolds, allowing for ample room for compression despite addition of stiff inorganic material. Mechanical testing was undergone in two phases, first with a 1kN electromechanical tester, which noted no difference modulus between scaffolds (data not shown). Further observation was undergone with atomic force microscopy to observe change in local stiffness of the individual nanofibers; upon this investigation, PCL/HA-3D scaffolds showed a significant increase in Young's modulus from 10.4±3.2 KPa to 38.6±11.4 KPa after both steps of SBF treatment ($P < 0.05$).

### 3.4 Protein and small molecule incorporation

To visualize protein and small molecule incorporation into HA layers, confocal microscopy was utilized in conjunction with fluorescent dyes; Rhodamine B incorporated into first step SBF solution (Fig. 4A,D) and fluorescein isothiocyanate labelled bovine serum albumin (FITC-BSA) incorporated into the second step solution (Fig. 4B,E) were viewed individually and in combination (Fig. 4C,F). To observe overall HA and molecule penetration into the bulk of scaffolds, a 30μm cross section was constructed using 2μm thick slices and imaged in 3D using Olympus confocal software (Fig. 4, D–F); 3D images show a uniform coating of both steps including fluorescent molecules throughout the scaffold, indicating that the two-step SBF coating method may sufficiently load multiple drugs and/or small molecules into TISA-PCL/HA composite scaffolds for drug release.

### 3.5 BSA and Phenamil release from NF composite scaffolds

Release profiles of BSA and phenamil from TISA-PCL/HA scaffolds are shown in Fig. 5. Scaffolds were treated with 3mL volumes of step-2 SBF containing either BSA (0.1mg/mL) or phenamil (0.2 mg/mL), where roughly one third of total molecule mass was incorporated into each scaffold after freeze-drying. An initial burst release was observed from both groups of BSA (Fig. 5A), while the incorporated group followed with a sustained release up to 20 days during experimental period. This pattern was also reflected in time-lapse confocal imaging of BSA-FITC fluorescence (Fig. 5B); as fluorescence intensity rapidly dropped after 7d in the adsorbed group, suggesting a high percent of total adsorbed FITC-BSA had released very quickly, whereas intensity remained higher for up to 21days for the incorporated group, indicating the BSA-FITC remained in the scaffold for a longer duration before depletion. Phenamil release profile is also shown (Fig. 5C), where a similar release pattern was observed; high burst release from the adsorbed group followed by minimal sustained release, while the incorporated phenamil showed some burst release followed by a sustained release, tapering off after 10days.

### 3.6 Cell morphology on PCL and PCL/HA composite scaffolds

In order to study the effect on cell attachment and morphology on scaffolds, confocal imaging was employed to visualize cell nuclei and cytoskeletal spreading on neat PCL and PCL/HA composite scaffolds (Fig. 6). Similar intensity of cytoskeletal staining was

observed in both scaffolds after 24h of culture (Fig. 6 A,D), however after 72h there was a marked increase in intensity of the cytoskeleton in TISA/HA composite scaffolds (Fig. 6B,E), indicating more intense cytoskeletal spreading of stem cells after just a few days. Both scaffolds displayed similar nuclei density within scaffolds, indicating they both act as favorable seeding vessels after several days.

### 3.7 Osteogenic differentiation of C2C12 cells on PCL/HA scaffolds with adsorbed and incorporated phenamil

To study the effect of sustained phenamil release from HA-modified scaffolds on the osteogenic differentiation of C2C12 cells, early osteogenic marker ALP as quantitatively observed and multiple gene expression were analyzed. As an early osteogenic marker, ALP was observed from cells cultured in 24-well plates, where a PCL/HA scaffold with either surfaced adsorbed phenamil or HA-incorporated phenamil was placed into growth medium after 10 days. Treatment of scaffolds with 100 μg phenamil yielded a significant increase in the incorporated group after 10d over TISA/HA untreated scaffolds, but produced significant cell death in the adsorbed group, consistent with prior literature noticing high phenamil doses as cytotoxic (data not shown)[40]. After reducing phenamil treatment amount by tenfold, a significant increase in ALP activity was noted over TISA/HA untreated scaffolds in both adsorbed and incorporated groups (Fig. 7A), with a larger increase noted in the incorporated group. Showing similar trend to the ALP activity, quantitative gene expression analysis revealed significant increase in early marker Runx2 gene expression in the incorporated group (Fig.7B). Later gene marker osteocalcin did not see a significant increase in expression, ($p<0.05$) however a trending increase was noted in the incorporated group after 10 days (Fig. 7C). This is likely that as a mature osteoblast marker, this gene relative expression would likely increase further with a longer culture time.[41]

## 4. Discussion

PCL-TISA scaffolds have shown some improved bioactivity through HA crystallization either via blends with PLA or use of very highly concentrated precipitation methods, yet the relative bioinert qualities of PCL still remain a concern.[21, 22] HA is a robust bone-like mineral capable of improving osteogenic differentiation of stem cells through its mimicking of the chemical environment of endogenous bone, as well as increasing the mechanical strength of many biomaterials.[42, 43] Additionally, its ability to encapsulate and protect growth factors for drug release is an increasingly studied niche in biomaterials-based drug-delivery platforms.[44] The SBF method for apatite deposition utilizes physiological mimicking conditions (i.e. room temperature, neutral pH) with no organic solvents, allowing it to maintain and protect activity of growth factors as a co-precipitation strategy. In our previous work, HA crystal deposition presented as individual crystals scattered within the scaffold fibers, a factor likely due to the high hydrophobicity of PCL, making it difficult for direct crystal growth on fibers to occur.[22] This work utilizes a two-step deposition strategy, with a first-step nucleating phase to prime the nanofibers for uniform crystalline growth in a second-step crystal propagating solution. As seen under SEM, nanofibers could be evenly and completely coated in 3D space while maintaining fibrous morphology at no observable cost of porosity. A two-step HA coating method is also desirable to incorporate multiple

drugs for simultaneous release, as single drug release is limited in ability to recapitulate the extended, multiple growth factor system presented in endogenous bone repair.[26, 27]

Mechanical observation in our previous research revealed TISA process could be used to generate highly elastic PCL-3D scaffolds, a property that was suggested to guide natural-mimicking endochondral ossification repair process of bone regeneration.[23] In this work, we find that after functionalization with HA, PCL-TISA composite scaffolds retain much of their elasticity, while seeing a significant increase in local mechanical strength as seen via AFM. As reported previously, mechanical strength is a contributor to osteogenic stem cell differentiation, as cells respond to their mechanical environment during differentiation.[45] This dual elasticity + high local mechanical strength could be attributed to the composite nature of the scaffolds[46, 47]; PCL-TISA by itself is highly elastic and with addition of mineral HA the local mechanical strength could be significantly strengthened without compromising the elasticity of the PCL matrix. Additionally, a tailored treatment profile (SBF strength/duration) allowed us to control the HA coating density as to not interrupt the porous morphology of scaffolds, likely another factor allowing scaffolds to retain their elastic properties. Maintaining porous morphology is also critical as it allows for movement and penetration of cells and incorporated/endogenous growth factors into the bulk of the scaffolds.[48, 49]

In our previous work, PCL scaffolds adopted a biomimicking niche with bone-like HA for osteogenic improvement, and simultaneously adsorbed phenamil to directly improve BMP2 signaling pathway.[22] It was noted that BMP2-induced bone formation could be further improved with a sustained drug release profile, as adsorbed burst release alone is limited in its osteogenic capabilities. Stem cell response *in vitro* noted significant improvement in ALP activity and Runx2 gene expression in scaffolds with incorporated phenamil versus the physically adsorbed group, as compared to PCL/HA scaffolds with no phenamil present. As also seen in the phenamil release curves, adsorbed group saw limited phenamil release occurring after the burst phase of 24h, whereas incorporated group possessed sustained release up to the experimental time of 10 days. This could simply be attributed to the sustained release of phenamil providing a stronger osteogenic niche than only a burst release profile without longer-term application.

PCL/HA-TISA scaffolds were able to simultaneously incorporate and release multiple and varied factors (i.e. small molecules and proteins), which demonstrate future capability of this technique to be expanded to utilize more specific factors for bone tissue engineering. Additional studies tailoring the amounts and types of drugs in encapsulation for modified release profiles may yield further improved osteogenic capabilities of the TISA scaffolds. Also noted in previous research and our prior work,[22, 32, 33], phenamil alone is insufficient for generation of new bone *in vivo.* Further strategies including animal studies with controlled release of both phenamil and BMP2 in tandem could also be a route for further improvement.

## 5. Conclusions

This research describes a novel, highly elastic biomimetic scaffold capable of multiple drug release for bone tissue engineering. PCL scaffolds adopted from the innovative TISA method remained highly elastic even after the fiber-localized multiple layer HA coating functionalized the surface of the 3D nanofibrous matrix. Scaffolds demonstrated capability of encapsulating multiple drugs for release, and studies using the BMP2 signaling agonist small molecule phenamil showed improved osteogenic differentiation profile of C2C12 cells with incorporated drug as compared to physically adsorbed molecules. Overall, these results suggest the PCL/HA composite scaffolds could be used as a press-fit scaffold biomaterial for drug delivery fit for bone tissue engineering.

## ACKNOWLDEGMENTS

This work was supported by the startup funds from the Department of Biomedical Engineering, University of South Dakota, the National Science Foundation/EPSCoR (Award Number: IIA-1335423), and the National Institute of Dental & Craniofacial Research of the National Institutes of Health under Award Numbers R01DE029159 and T90DE023520. The content is solely the responsibility of the authors and does not necessarily represent the official views of the National Institutes of Health.

## References

(1). De Long WG Jr.; Einhorn TA; Koval K; McKee M; Smith W; Sanders R; Watson T, Bone grafts and bone graft substitutes in orthopaedic trauma surgery. A critical analysis. The Journal of bone and joint surgery. American volume 2007, 89 (3), 649–58. [PubMed: 17332116]

(2). Hutmacher DW, Scaffolds in tissue engineering bone and cartilage. Biomaterials 2000, 21 (24), 2529–2543. [PubMed: 11071603]

(3). Bose S; Vahabzadeh S; Bandyopadhyay A, Bone tissue engineering using 3D printing. Materials Today 2013, 16 (12), 496–504.

(4). De Mori A; Pena Fernandez M; Blunn G; Tozzi G; Roldo M, 3D Printing and Electrospinning of Composite Hydrogels for Cartilage and Bone Tissue Engineering. Polymers 2018, 10 (3).

(5). De Nardo L; De Cicco S; Jovenitti M; Tanzi M; Farè S, Shape Memory Polymer Porous Structures for Mini-Invasive Surgical Procedures. 2006; p 539–544.

(6). Zhang D; George OJ; Petersen KM; Jimenez-Vergara AC; Hahn MS; Grunlan MA, A bioactive “self-fitting” shape memory polymer scaffold with potential to treat cranio-maxillo facial bone defects. Acta biomaterialia 2014, 10 (11), 4597–4605. [PubMed: 25063999]

(7). Kai D; P Prabhakaran M; Chan BQY; Liow S. s.; Ramakrishna S; Xu F; Loh XJ, Elastic poly(ε -caprolactone)-polydimethylsiloxane copolymer fibers with shape memory effect for bone tissue engineering. 2016; Vol. 11, p 015007.

(8). Alsberg E; Anderson KW; Albeiruti A; Franceschi RT; Mooney DJ, Cell-interactive alginate hydrogels for bone tissue engineering. Journal of dental research 2001, 80 (11), 2025–9. [PubMed: 11759015]

(9). Slaughter BV; Khurshid SS; Fisher OZ; Khademhosseini A; Peppas NA, Hydrogels in regenerative medicine. Advanced materials (Deerfield Beach, Fla.) 2009, 21 (32–33), 3307–29.

(10). Lutolf MP; Lauer-Fields JL; Schmoekel HG; Metters AT; Weber FE; Fields GB; Hubbell JA, Synthetic matrix metalloproteinase-sensitive hydrogels for the conduction of tissue regeneration: Engineering cell-invasion characteristics. Proceedings of the National Academy of Sciences 2003, 100 (9), 5413.

(11). Burdick JA; Anseth KS, Photoencapsulation of osteoblasts in injectable RGD-modified PEG hydrogels for bone tissue engineering. Biomaterials 2002, 23 (22), 4315–4323. [PubMed: 12219821]

(12). Gibbs DM; Black CR; Dawson JI; Oreffo RO, A review of hydrogel use in fracture healing and bone regeneration. Journal of tissue engineering and regenerative medicine 2016, 10 (3), 187–98. [PubMed: 25491789]

(13). Xu T; Miszuk JM; Zhao Y; Sun H; Fong H, Electrospun polycaprolactone 3D nanofibrous scaffold with interconnected and hierarchically structured pores for bone tissue engineering. Advanced healthcare materials 2015, 4 (15), 2238–46. [PubMed: 26332611]

(14). Hu C; Zhang T; Ren B; Deng Z; Cai L; Lei J; Ping A, Effect of vacuum-assisted closure combined with open bone grafting to promote rabbit bone graft vascularization. Medical science monitor : international medical journal of experimental and clinical research 2015, 21, 1200–6. [PubMed: 25913359]

(15). Lappalainen OP; Korpi R; Haapea M; Korpi J; Ylikontiola LP; Kallio-Pulkkinen S; Serlo WS; Lehenkari P; Sándor GK, Healing of rabbit calvarial critical-sized defects using autogenous bone grafts and fibrin glue. Child's nervous system : ChNS : official journal of the International Society for Pediatric Neurosurgery 2015, 31 (4), 581–7.

(16). Kock NB; Van Susante JLC; Buma P; Van Kampen A; Verdonschot N, Press-fit stability of an osteochondral autograft: influence of different plug length and perfect depth alignment. Acta Orthopaedica 2006, 77 (3), 422–428. [PubMed: 16819681]

(17). Wang L; Cao L; Shansky J; Wang Z; Mooney D; Vandenburgh H, Minimally Invasive Approach to the Repair of Injured Skeletal Muscle With a Shape-memory Scaffold. Molecular Therapy 2014, 22 (8), 1441–1449. [PubMed: 24769909]

(18). Zhang D; Wu X; Chen J; Lin K, The development of collagen based composite scaffolds for bone regeneration. Bioactive materials 2018, 3 (1), 129–138. [PubMed: 29744450]

(19). Wu Z; Meng Z; Wu Q; Zeng D; Guo Z; Yao J; Bian Y; Gu Y; Cheng S; Peng L; Zhao Y, Biomimetic and osteogenic 3D silk fibroin composite scaffolds with nano MgO and mineralized hydroxyapatite for bone regeneration. J Tissue Eng 2020, 11, 2041731420967791.

(20). Chahal AS; Schweikle M; Lian AM; Reseland JE; Haugen HJ; Tiainen H, Osteogenic potential of poly(ethylene glycol)-amorphous calcium phosphate composites on human mesenchymal stem cells. J Tissue Eng 2020, 11, 2041731420926840.

(21). Yao Q; Cosme JG; Xu T; Miszuk JM; Picciani PH; Fong H; Sun H, Three dimensional electrospun PCL/PLA blend nanofibrous scaffolds with significantly improved stem cells osteogenic differentiation and cranial bone formation. Biomaterials 2017, 115, 115–127. [PubMed: 27886552]

(22). Miszuk JM; Xu T; Yao Q; Fang F; Childs JD; Hong Z; Tao J; Fong H; Sun H, Functionalization of PCL-3D electrospun nanofibrous scaffolds for improved BMP2-induced bone formation. Applied Materials Today 2018, 10, 194–202. [PubMed: 29577064]

(23). Xu T; Yao Q; Miszuk JM; Sanyour HJ; Hong Z; Sun H; Fong H, Tailoring weight ratio of PCL/PLA in electrospun three-dimensional nanofibrous scaffolds and the effect on osteogenic differentiation of stem cells. Colloids and surfaces. B, Biointerfaces 2018, 171, 31–39. [PubMed: 30005288]

(24). Richardson TP; Peters MC; Ennett AB; Mooney DJ, Polymeric system for dual growth factor delivery. Nature biotechnology 2001, 19 (11), 1029–34.

(25). Lutolf MP; Hubbell JA, Synthetic biomaterials as instructive extracellular microenvironments for morphogenesis in tissue engineering. Nat Biotechnol 2005, 23 (1), 47–55. [PubMed: 15637621]

(26). Kim YH; Tabata Y, Dual-controlled release system of drugs for bone regeneration. Advanced drug delivery reviews 2015, 94 (1), 28–40. [PubMed: 26079284]

(27). Bagherifard S, Mediating bone regeneration by means of drug eluting implants: From passive to smart strategies. Materials science & engineering. C, Materials for biological applications 2017, 71, 1241–1252. [PubMed: 27987680]

(28). Hankenson KD; Gagne K; Shaughnessy M, Extracellular signaling molecules to promote fracture healing and bone regeneration. Advanced drug delivery reviews 2015, 94, 3–12. [PubMed: 26428617]

(29). Pearson HB; Mason DE; Kegelman CD; Zhao L; Dawahare JH; Kacena MA; Boerckel JD, Effects of BMP-2 on neovascularization during large bone defect regeneration. Tissue engineering. Part A 2019.

(30). Haidar ZS; Hamdy RC; Tabrizian M, Delivery of recombinant bone morphogenetic proteins for bone regeneration and repair. Part A: Current challenges in BMP delivery. Biotechnology letters 2009, 31 (12), 1817–24. [PubMed: 19690804]

(31). Bessa PC; Casal M; Reis RL, Bone morphogenetic proteins in tissue engineering: the road from laboratory to clinic, part II (BMP delivery). Journal of tissue engineering and regenerative medicine 2008, 2 (2–3), 81–96. [PubMed: 18383454]

(32). Fan J; Guo M; Im CS; Pi-Anfruns J; Cui ZK; Kim S; Wu BM; Aghaloo TL; Lee M, Enhanced Mandibular Bone Repair by Combined Treatment of Bone Morphogenetic Protein 2 and Small-Molecule Phenamil. Tissue engineering. Part A 2017, 23 (5–6), 195–207. [PubMed: 27771997]

(33). Fan J; Im CS; Cui ZK; Guo M; Bezouglaia O; Fartash A; Lee JY; Nguyen J; Wu BM; Aghaloo T; Lee M, Delivery of Phenamil Enhances BMP-2-Induced Osteogenic Differentiation of Adipose-Derived Stem Cells and Bone Formation in Calvarial Defects. Tissue engineering. Part A 2015, 21 (13–14), 2053–65. [PubMed: 25869476]

(34). Park KW; Waki H; Kim WK; Davies BS; Young SG; Parhami F; Tontonoz P, The small molecule phenamil induces osteoblast differentiation and mineralization. Molecular and cellular biology 2009, 29 (14), 3905–14. [PubMed: 19433444]

(35). Lo KW; Kan HM; Laurencin CT, Short-term administration of small molecule phenamil induced a protracted osteogenic effect on osteoblast-like MC3T3-E1 cells. Journal of tissue engineering and regenerative medicine 2016, 10 (6), 518–26. [PubMed: 23913855]

(36). Wu G; Liu Y; Iizuka T; Hunziker EB, Biomimetic coating of organic polymers with a protein-functionalized layer of calcium phosphate: the surface properties of the carrier influence neither the coating characteristics nor the incorporation mechanism or release kinetics of the protein. Tissue engineering. Part C, Methods 2010, 16 (6), 1255–65. [PubMed: 20196638]

(37). Yao Q; Liu Y; Selvaratnam B; Koodali RT; Sun H, Mesoporous silicate nanoparticles/3D nanofibrous scaffold-mediated dual-drug delivery for bone tissue engineering. Journal of controlled release : official journal of the Controlled Release Society 2018, 279, 69–78. [PubMed: 29649529]

(38). Yao Q; Sandhurst ES; Liu Y; Sun H, BBP-Functionalized Biomimetic Nanofibrous Scaffold Can Capture BMP2 and Promote Osteogenic Differentiation. Journal of materials chemistry. B 2017, 5 (26), 5196–5205. [PubMed: 29250330]

(39). Stanić V; Janaćković D; Dimitrijević S; Tanasković SB; Mitrić M; Pavlović MS; Krstić A; Jovanović D; Raičević S, Synthesis of antimicrobial monophase silver-doped hydroxyapatite nanopowders for bone tissue engineering. Applied Surface Science 2011, 257 (9), 4510–4518.

(40). Brun V; Guillaume C; Mechiche Alami S; Josse J; Jing J; Draux F; Bouthors S; Laurent-Maquin D; Gangloff SC; Kerdjoudj H; Velard F, Chitosan/hydroxyapatite hybrid scaffold for bone tissue engineering. Bio-medical materials and engineering 2014, 24 (1 Suppl), 63–73. [PubMed: 24928919]

(41). Hassan MQ; Tare RS; Lee SH; Mandeville M; Morasso MI; Javed A; van Wijnen AJ; Stein JL; Stein GS; Lian JB, BMP2 commitment to the osteogenic lineage involves activation of Runx2 by DLX3 and a homeodomain transcriptional network. The Journal of biological chemistry 2006, 281 (52), 40515–26. [PubMed: 17060321]

(42). Li B; Kan L; Zhang X; Li J; Li R; Gui Q; Qiu D; He F; Ma N; Wang Y; Wei H, Biomimetic Bone-like Hydroxyapatite by Mineralization on Supramolecular Porous Fiber Networks. Langmuir : the ACS journal of surfaces and colloids 2017, 33 (34), 8493–8502. [PubMed: 28803478]

(43). Zima A, Hydroxyapatite-chitosan based bioactive hybrid biomaterials with improved mechanical strength. Spectrochimica acta. Part A, Molecular and biomolecular spectroscopy 2018, 193, 175–184.

(44). Basargan T; Erdol-Aydin N; Nasun-Saygili G, Hydroxyapatite-chitosan biocomposites synthesized in the simulated body fluid and their drug loading studies. Journal of materials science. Materials in medicine 2017, 28 (11), 180. [PubMed: 28986683]

(45). Sun H; Zhu F; Hu Q; Krebsbach PH, Controlling stem cell-mediated bone regeneration through tailored mechanical properties of collagen scaffolds. Biomaterials 2014, 35 (4), 1176–84. [PubMed: 24211076]

(46). Kim H-W; Knowles JC; Kim H-E, Hydroxyapatite/poly(ε-caprolactone) composite coatings on hydroxyapatite porous bone scaffold for drug delivery. Biomaterials 2004, 25 (7), 1279–1287. [PubMed: 14643602]

(47). Roohani-Esfahani SI; Nouri-Khorasani S; Lu Z; Appleyard R; Zreiqat H, The influence hydroxyapatite nanoparticle shape and size on the properties of biphasic calcium phosphate scaffolds coated with hydroxyapatite-PCL composites. Biomaterials 2010, 31 (21), 5498–509. [PubMed: 20398935]

(48). Karageorgiou V; Kaplan D, Porosity of 3D biomaterial scaffolds and osteogenesis. Biomaterials 2005, 26 (27), 5474–91. [PubMed: 15860204]

(49). Rezwan K; Chen QZ; Blaker JJ; Boccaccini AR, Biodegradable and bioactive porous polymer/inorganic composite scaffolds for bone tissue engineering. Biomaterials 2006, 27 (18), 3413–3431. [PubMed: 16504284]

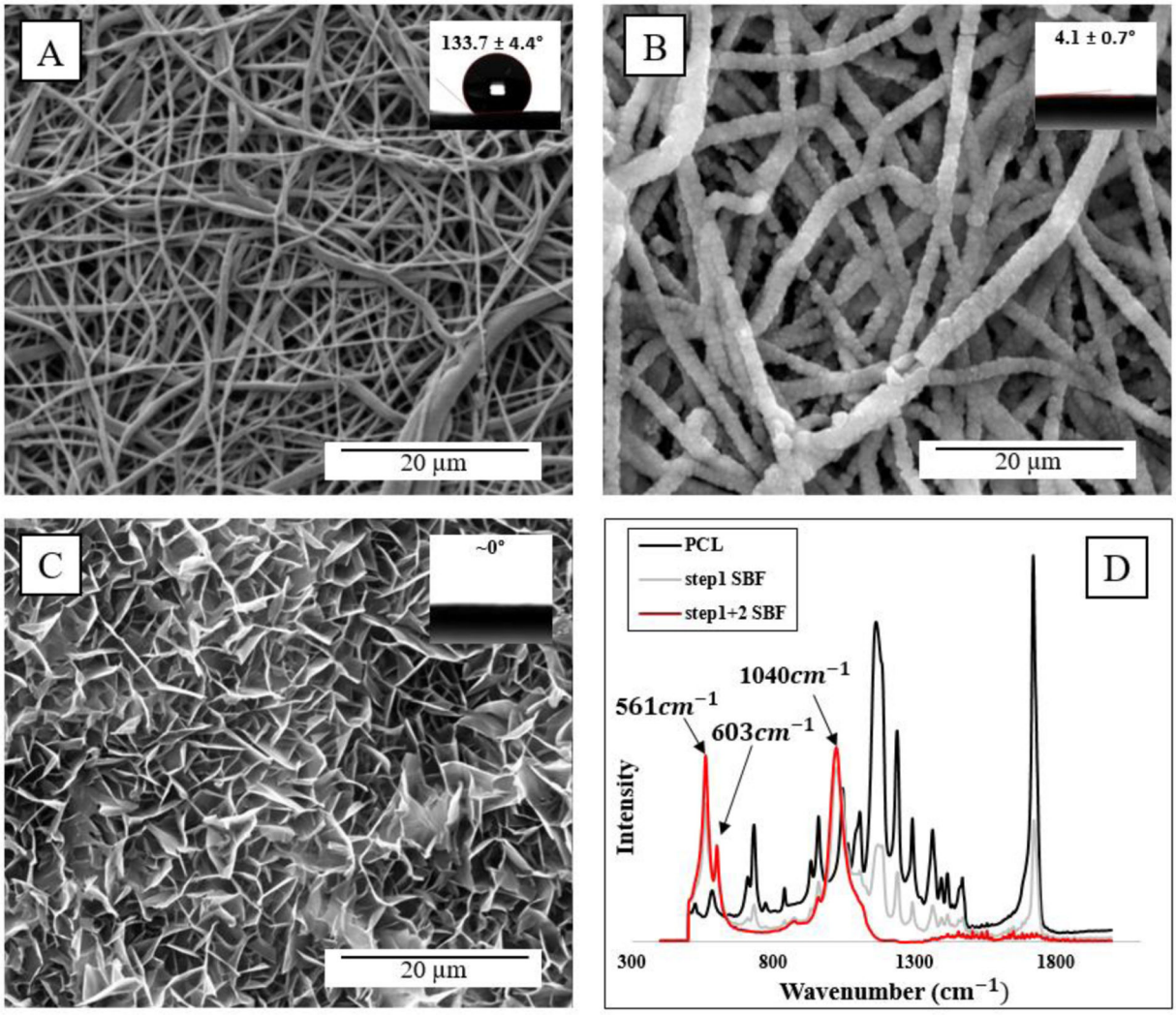


**Fig. 1.**

SEM morphology and contact angles of NF PCL mats before soaking in either SBF step (A), after step 1 (B), and after both steps (C). ATR spectra of NF PCL mats prior to and after SBF treatment (D).

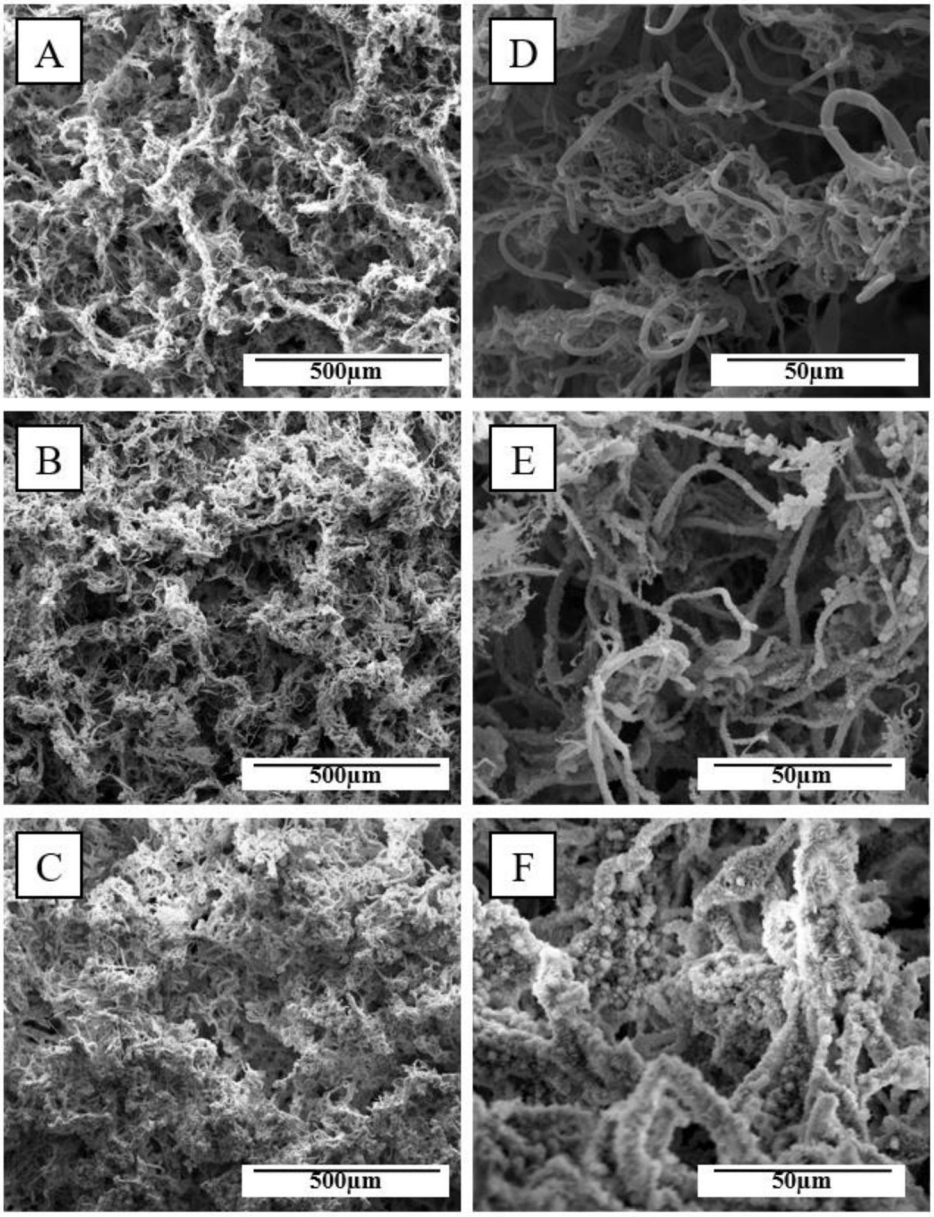


**Fig. 2.**

SEM images showing representative morphologies of PCL-3D scaffolds in low (A-C) and high (D-F) magnification. Rows top to bottom visualize neat PCL, step1 coating, and step2 SBF coating.

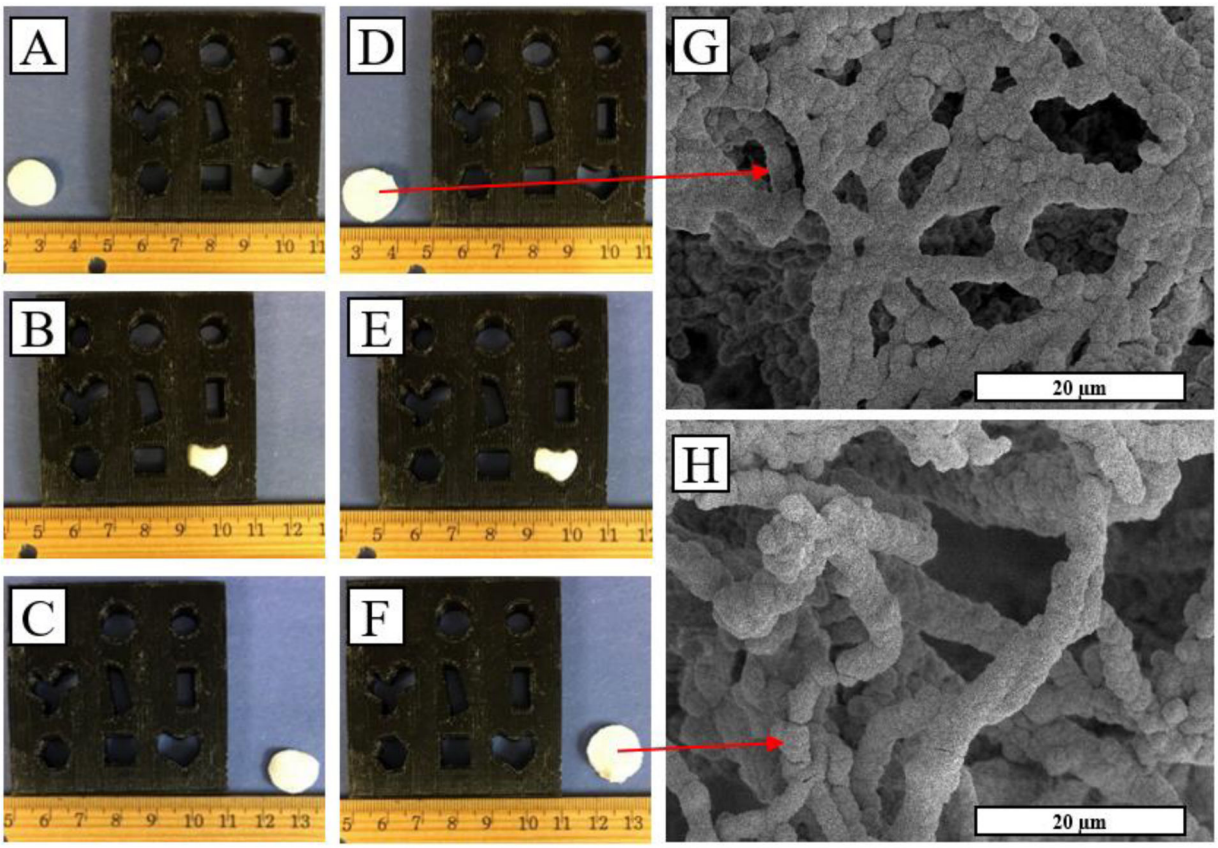


**Fig. 3.**

TISA-PCL prior to compression (A) was press-fit into a defect for 10 minutes (B) and then removed and rested for 60sec to resume its original shape (C). The same process was repeated for TISA-PCL/HA composite scaffold (D-F). SEM images of TISA/PCL-HA scaffolds show nanofiber morphology prior to (G) and after (H) compression.

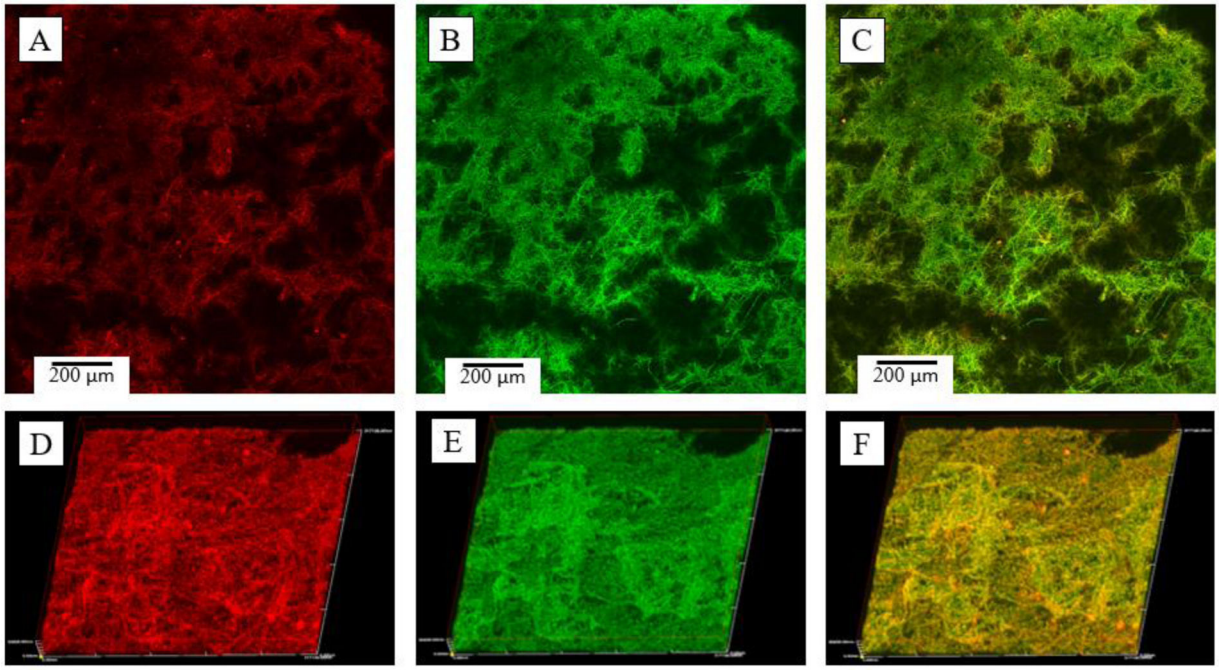


**Fig. 4.**

Confocal imaging of PCL/HA scaffolds of individual layers (A-C) and 30 µm 3D-cross sections (D-F). Fluorescent dyes were introduced into step 1 SBF with rhodamine B (red) and FITC-BSA (green).

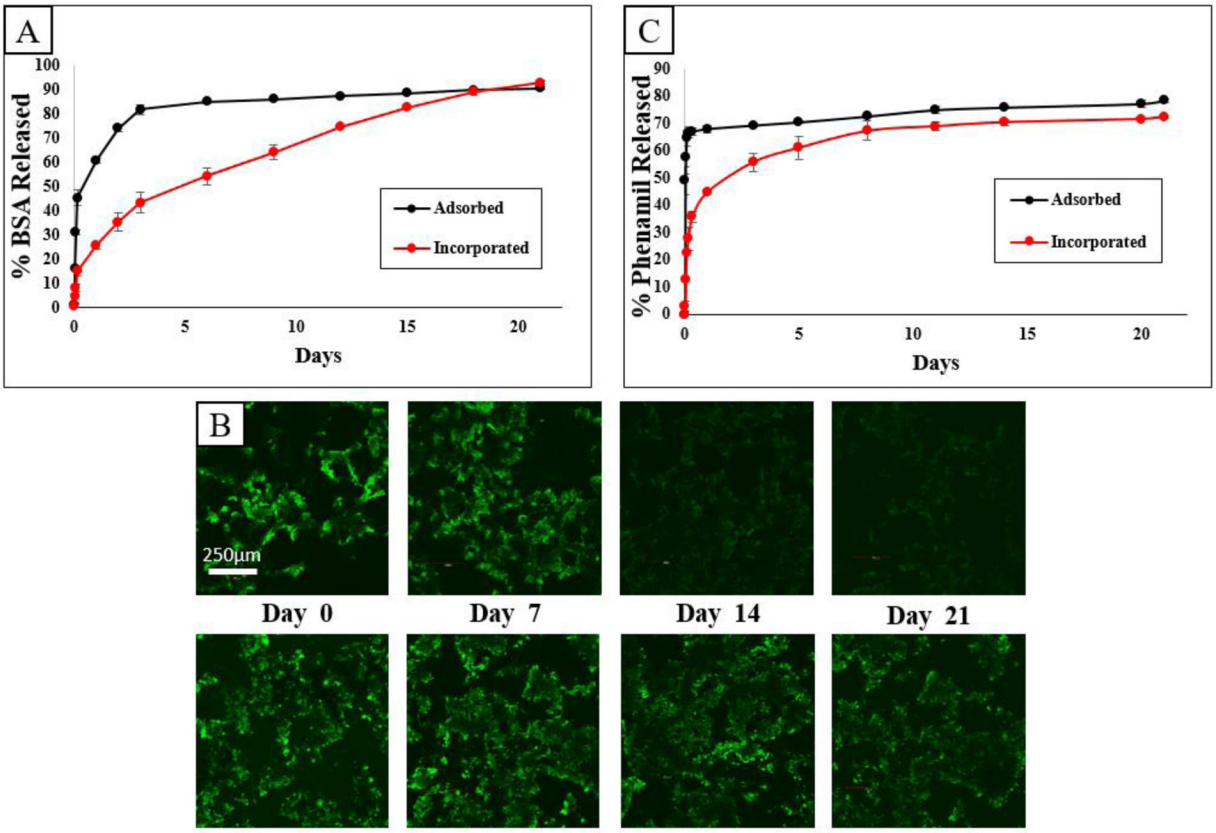


**Fig. 5.**

Release profile of BSA from scaffolds (A) visualized as total percentage released. Fluorescence time-lapse of adsorbed group (B, top row) and incorporated group (B, bottom row). Release profile of phenamil from scaffolds as total percent released (C).

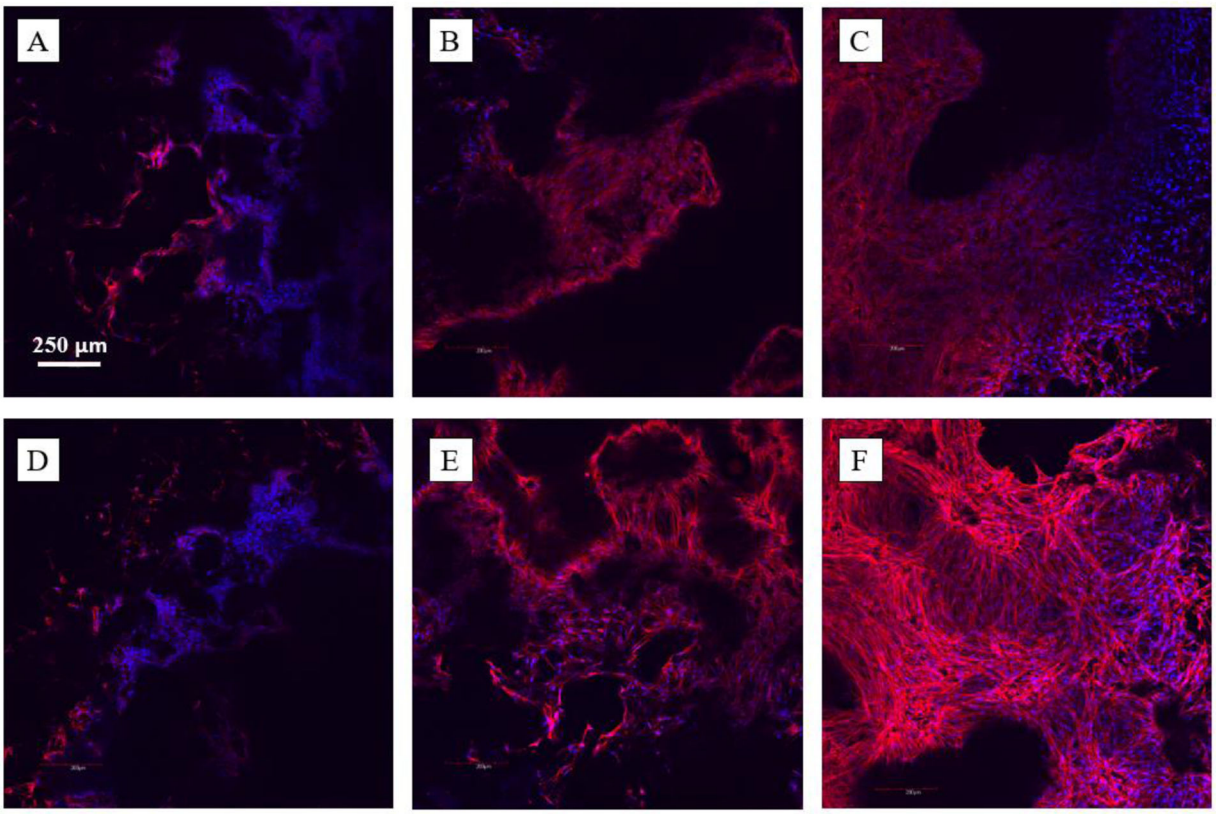


**Fig. 6.**

C2C12 morphologies on TISA (top row) and TISA/HA composite (bottom row) scaffolds, after 24h (A, D) and 72h (B, E) of culture. C and F show a 100µm z-stack of cell morphologies after 72h of culture in each scaffold.

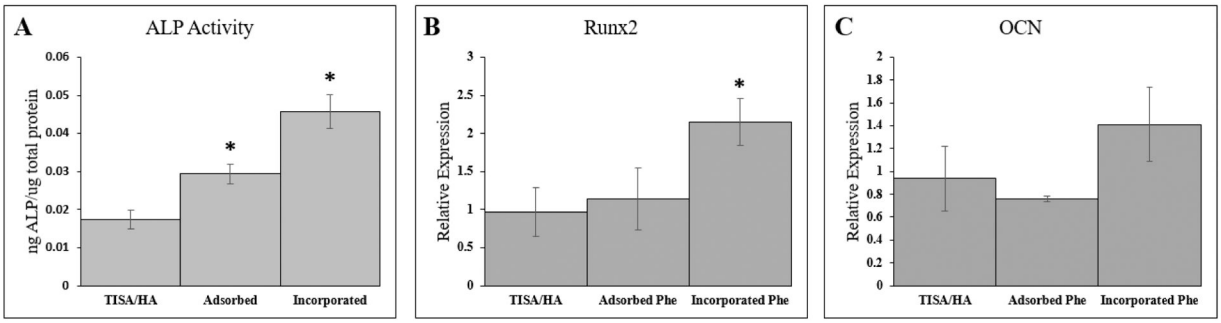


**Fig. 7.**

ALP activity of C2C12 cells cultured on dishes after 10days in presence of TISA/HA scaffolds with or without adsorbed/incorporated phenamil present (A). Osteogenic gene markers Runx2 (B) and OCN (C) were measured by real-time PCR assays after culturing for 10 days within TISA/HA scaffolds. Data are expressed as mean ± SD (n=3).